Int J Earth Sci (Geol Rundsch) (2005) 94: 8–23
DOI 10.1007/s00531-004-0445-0

ORIGINAL PAPER

Wolfgang Siebel · Ulrich Blaha · Fukun Chen
Johann Rohrmüller

Geochronology and geochemistry of a dyke–host rock association and implications for the formation of the Bavarian Pfahl shear zone, Bohemian Massif

Received: 2 February 2004 / Accepted: 14 September 2004 / Published online: 19 November 2004

Abstract To place constraints on the formation and deformation history of the major Variscan shear zone in the Bavarian Forest, Bavarian Pfahl zone, SW Bohemian Massif, granitic dykes and their feldspar-phyric massive host rock (so-called "palite"), zircons were dated by the U–Pb isotope dilution and Pb-evaporation methods. The dated samples comprise two host rocks and four dykes from a K-rich calc-alkaline complex adjoining the SW part of the Bavarian Pfahl shear zone. The palites, which appear to be the oldest magmatic rocks emplaced in the shear zone, yield ages of 334 ± 3, 334.5 ± 1.1 Ma (average $^{207}Pb/^{206}Pb$-evaporation zircon ages) and 327–342 Ma (range of U/Pb zircon ages) suggesting a Lower Carboniferous age for the initiation of the Pfahl zone. Absence of inherited older cores in all investigated zircons indicates that incorporation of crustal zircon material has played virtually no role or that the melting temperature was very high. Determination of the dyke emplacement age is complicated by partial Pb-loss in most of the fractions analysed. This Pb-loss can be ascribed to higher U content of the dyke zircons compared to those from host rock. Upper discordia intercept ages of the different dykes range from 322 ± 5 to 331 ± 9 Ma. The dykes are pre- to synkinematic with respect to penetrative regional mylonitisation along the Pfahl zone, and the upper intercept ages provide a maximum age for this tectonic event.

Keywords Bavarian Pfahl · Granitic dyke · Palite · Shear zone · U–Pb zircon dating

W. Siebel (✉) · U. Blaha
Institut für Geowissenschaften,
Universität Tübingen, Wilhelmstraße 56,
72074 Tübingen, Germany
E-mail: wolfgang.siebel@uni-tuebingen.de
Tel.: +49-7071-2974991
Fax: +49-7071-295713

F. Chen
Laboratory for Radiogenic Isotope Geochemistry,
Institute of Geology and Geophysics,
Chinese Academy of Sciences, 100029 Beijing, China

J. Rohrmüller
Bayerisches Geologisches Landesamt,
Außenstelle Marktredwitz, Leopoldstraße 30,
95615 Marktredwitz, Germany

Introduction

Dyke rocks are useful geological time markers for the late or post-deformational stage of magmatic activity in orogenic belts (Crowley 1999) or reactivation of consolidated orogens (Košler et al. 2001). Besides, they are also candidates for dating extensional events like continental break up (White et al. 1987) or intra-continental rifting (Amelin et al. 1995; Kamo et al. 1995). Given their small volume, dykes are fast-cooling intrusives and even isotopic systems with low closure temperatures (e.g. K–Ar) can portray the age of dyke formation (e.g. Anczkiewicz et al. 2001; Košler et al. 2001). In zones of crustal reactivation, e.g. shear zones, the K–Ar and even the U–Pb mineral systems can be disturbed or reset by later reheating (e.g. Mulch et al. 2002). Within such zones, that have an important control in focussing and accommodating magma emplacement (e.g. Weinberg 1996; Schneider et al. 1999), the U–Pb system can still provide appropriate benchmarks for the crystallisation age, provided the dykes contain accessory U-bearing minerals with high closure temperature such as zircon.

The recent discovery of numerous granitic dykes in the Bavarian Pfahl shear zone, Bohemian Massif, European Variscides, was an unexpected result of a detailed geological mapping survey undertaken by the second author. The dykes intrude a peculiar rock-type of prevailing granodioritic composition with varying amounts of alkali-feldspar megacrysts, known as *palite* (Frentzel 1911). The dykes are characterised by WNW striking fabrics that are the result of multiple episodes of deformation, the age of which was controversially discussed by Thiele (1961), Dvorak (1985) and Brandmayr

et al. (1995). The dykes are mylonitised to various extents and are therefore important time markers that can be used to constrain the age of the penetrative mylonitisation event along the Pfahl zone. Here, we report the results of a U–Pb isotope dilution and Pb-evaporation zircon study of the dyke–host rock assemblage and discuss their geological significance. The data provide new information on the onset of the Pfahl formation and help to constrain the time of mylonitisation. Subsequent to reporting our geochronological results, we discuss the compositional relation between host rock and cross-cutting dykes.

Geological setting

The study area comprises a part of the Bavarian Pfahl zone (Fig. 1), a major shear zone within the southwestern part of the Bohemian Massif (Hofmann 1962; Brandmayr et al. 1995; Mattern 2001). The Pfahl zone represents a tectonic zone of persistent crustal weakness and, as such, provides a window into processes that control crustal reactivation. It strikes 120° and runs >150 km from the town of Schwarzenfeld in the Oberpfalz to Upper Austria (Fig. 1). It is parallel to a second crustal flaw, the Danubian shear zone, which is positioned ca. 30 km further SW (Fig. 1). Including NNE–SSW running shear zones in the southern Bohemian Massif, these zones belong to a conjugate shear zone system (Wallbrecher et al. 1992). Recently, it was argued that the shear zones formed during Silesian block interaction between Baltica and Western Europe (Mattern 1995, 2001). For the Pfahl shear zone, it is assumed that the rocks were initially displaced by dextral shearing and received a sinistral reactivation during the Rotliegend (Mattern 1995, 2001). According to Brandmayr et al. (1995), the metamorphic conditions in the shear zones reached amphibolite facies temperatures of up to 650°C. Evidence of dextral shear sense is preserved in mylonites and ultramylonites, and some of these rocks were transformed into cataclastic rocks during a subsequent phase of brittle deformation. In Permo-Triassic time, the fault system was reactivated and episodic influx of silica-rich fluids resulted in nearly vertical zones of Pfahlquartz precipitation (Ochotzky and Sandkühler 1914; Hegemann 1936; Hofmann 1962; Horn et al. 1986). The quartz was deposited from hydrothermal fluids in or in the proximity to the sheared zones in the temperature range from 280 to 120°C (Peucker-Ehrenbrink and Behr 1993).

In terms of rock lithologies, the Pfahl zone separates anatectic biotite-plagioclase gneisses (Perlgneise, sensu Fischer 1938, 1959) and K-feldspar-sillimanite gneisses on its southwestern side from migmatitic cordierite-sillimanite gneisses to the northeast. Both lithological units are part of the Drosendorf Monotonous series of the Moldanubian *sensu stricto* (Matte et al. 1990; Petrakakis 1997; Franke 2000). The rocks known as palites occur in

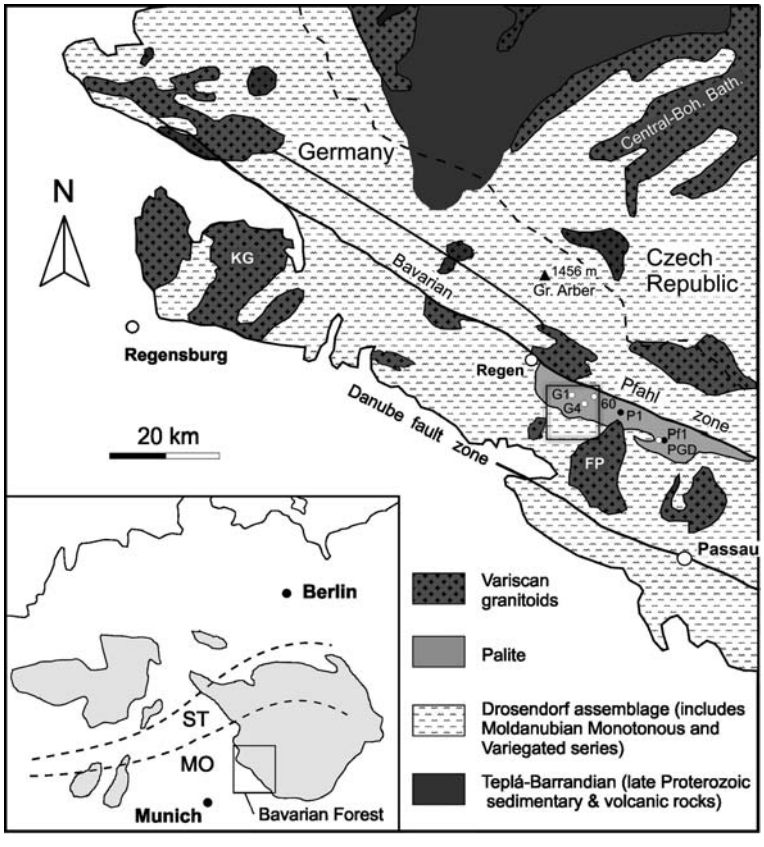

Fig. 1 Generalised geological map (simplified from Christinas et al. 1991) of the Bavarian Forest showing the Bavarian Pfahl shear zone, palite distribution and position of samples dated in this study (*filled circles* palites, *open circles* dykes). Additional samples taken for geochemical analyses originate from 1:25,000 geological map sheet "7145 Schöfweg" (area indicated by *square*) and their exact location is given in Table 1. Abbreviations: *ST* Saxothuringian zone, *MO* Moldanubian zone. *KG* Kristallgranit and *FP* Fürstenstein Pluton are Variscan granitoids mentioned in the text

a 5–7 km wide zone along the southwestern part of the Pfahl zone, beginning near the town of Regen and continuing southeastwards over a distance of > 50 km (Fig. 1). The most distinctive rock type is a coarse-grained, inequigranular granitoid of dominantly granodioritic composition, which often contains large megacrysts of K-feldspar, sometimes augen-shaped. Metabasites (gabbros, diorites and amphibolites) of various sizes (1–100 m) occur as enclaves or nodules in the palites (Steiner 1972; Christinas et al. 1991, own observation). According to Christinas et al. (1991), the coexistence of palites and mafic bodies is the result of mechanical mixing during intrusion.

Although several processes (magmatic, metamorphic and metasomatic) seem to have contributed to the formation of the palites, the rocks are generally considered by most authors to be dominantly of magmatic origin (Steiner 1972; Troll 1967; Köhler et al. 1989). Troll (1967) and Steiner (1969, 1972) presented a hypothesis which considers the K-feldspar megacrysts as a result of metasomatic formation. Metasomatic fluids are thought to have been derived from late-Variscan K-feldspar bearing granite intrusions. Whatever their exact origin, palites are witnesses of the complicated deformation history along the Pfahl zone. Their location parallel to the Pfahl zone suggests that the presence of this zone has exerted a structural control on their formation and geographic distribution.

At various localities, the palites are cross-cut by fine-grained aphyric granitic dykes. Some of these dykes show equigranular textures, but most of them are weakly to strongly deformed and possess a penetrative foliation (Figs. 2, 3). In contrast to the palites, the cross-cutting dykes do not contain K-feldspar megacrysts. Field mapping has proved that the granitic dykes mainly occur within the palites and their peripheral parts; no evidence on these dykes penetrating the surrounding paragneisses away from the palites has been found. There is a tendency for the dykes to parallel the Pfahl zone (Köhler et al. 1989, own observations) which means that they are linked to tectonic activity along this zone. To the southeast, the palites are intersected by coarse-grained K-feldspar granitic dykes (Steiner 1972). These rocks are undeformed and mainly restricted to the south-eastern part of the palite zone and have lower silica and higher Ti, Ca and Mg contents compared to the granitic dykes investigated in this study. Based on these discernible features, there seems to be no genetic link between these two types of dyke rocks.

Previous geochronology

Despite much research into various geological aspects of the Pfahl zone and the palites over the past 135 years (since the pioneering work of Gümbel 1868), the formation age of this peculiar rock-type is poorly constrained. Christinas et al.'s (1991) Rb–Sr dating was the only geochronological study on the palites before our investigation. Rb–Sr whole-rock isotope analyses from nine palite samples yield an isochron with an age of 474 ± 18 Ma. Based on the low initial $^{87}Sr/^{86}Sr$-value of 0.7051, Christinas et al. (1991) argued that the palite magma was derived from an upper mantle source. According to these authors, the Rb–Sr system was apparently not disturbed by the tectonic events along the Pfahl zone or by magma mixing, and the age was regarded as Ordovician emplacement age. Rb–Sr mineral isochrons (biotite and apatite) of palites from the Saunstein quarry, north of the town of Schönberg, provide cooling ages between 315 and 303 Ma (mean: 310 ± 7 Ma). Muscovite-whole rock Rb–Sr isotope data on a granitic dyke rock from this quarry give an age of 316 ± 6 Ma and an initial $^{87}Sr/^{86}Sr$ isotope ratio of 0.7358 ± 0.0001 (all data from Christinas et al. 1991). This age was interpreted as the minimum age of regional mylonitisation. Both newly grown and porphyroclastic muscovite grains from the southeastern part of the Pfahl and Danube shear zones yield $^{40}Ar/^{39}Ar$ ages as young as ca. 287 Ma, indicating that mylonitisation lasted until Permian times (Brandmayr et al. 1995). Brittle extensional movement in the NNE striking Blanice-Kaplice-Rödl shear zone, southern Bohemia, has been constrained at 270 Ma by $^{40}Ar/^{39}Ar$ amphibole dating

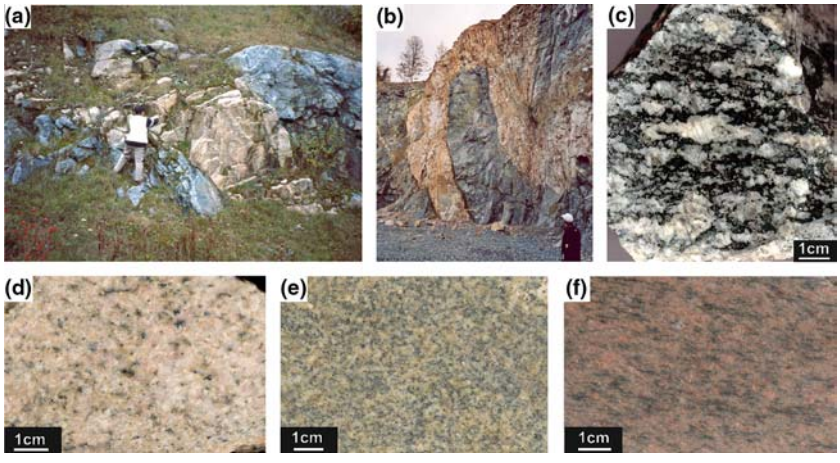

Fig. 2 Examples of dyke outcrops and rock types **a** Road-cut at the B12 between Kumreut and Garham, revealing a pink granitic dyke cutting through dark-grey palite, **b** dyke enclosing a large fragment of palite, Saunstein quarry; **c** polished rock slab showing palite with prominent gneissic foliation (sample P1) dated in this study; **d–f** close-up views of dyke samples PGD (**d**), G4 (**e**) and 60 (**f**) dated in this study

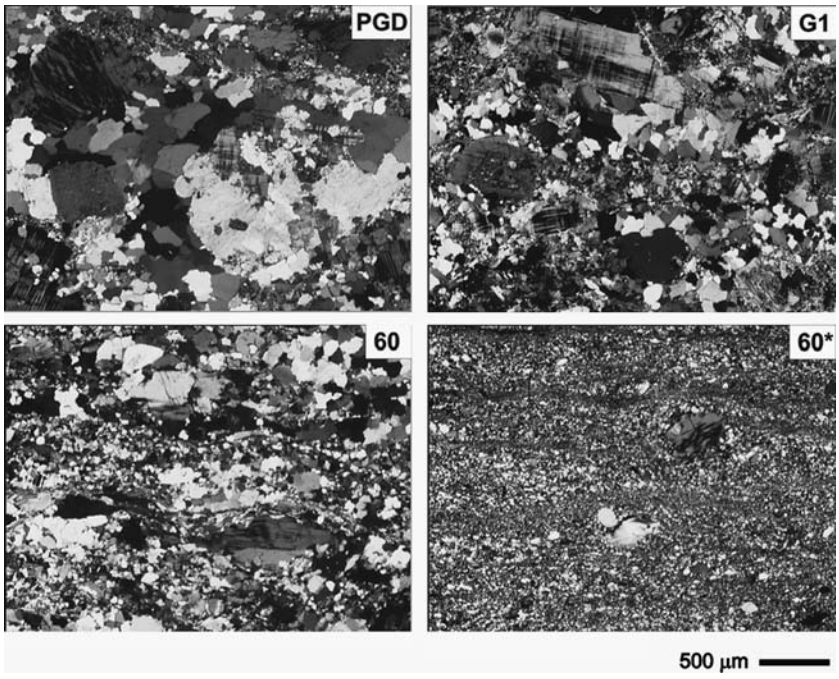

Fig. 3 Thin section photographs illustrating microtextures of various granitic dykes. All photographs taken at the same magnification (2.5×) and at plane polarised light; samples are arranged according to increasing grain-size reduction; **a** dyke PGD—nearly undeformed with primary magmatic crystallisation texture, **b** dyke G1 showing incipient mylonitisation, **c** mylonite (sample 60), fine-grained and containing strongly aligned minerals, **d** dyke 60*, i.e. the margin of dyke 60 dramatically changed by shearing and recrystallisation and transformed into ultramylonite. Matrix is very fine grained, mostly made up of quartz and banding is more intense. Bright streaks are strung-out bundles of mica flakes. Two rounded porphyroclasts appear isolated in the quartz and mica matrix

of a microgranodioritic dyke (Košler et al. 2001). Horn et al. (1986) reported a Rb–Sr isochron age for six quartz samples from the Bavarian Pfahl of 247 ± 21 Ma, suggesting that hydrothermal quartz crystallisation occurred during the Lower Triassic and, based on an initial $^{87}Sr/^{86}Sr$ isotope ratio of 0.7133 ± 0.0007, the authors inferred an upper crustal origin of the mineralisation.

Analytical techniques

Rock samples (5–8 kg) were prepared for geochemical analyses by jaw crushing and pulverising in disk mills and ceramic disk grinders. Major elements (SiO_2, TiO_2, Al_2O_3, Fe_2O_3, MnO, MgO, CaO, Na_2O, K_2O and P_2O_5), selected trace elements (Sr, Ba, Rb, Zr, Y, Th and Pb) and selected rare-earth elements (REEs: La, Ce, Nd, Sm, Eu and Yb) were analysed using X-ray fluorescence (XRF) spectrometry on a Bruker AXS S4 Pioneer spectrometer. The relative standard deviations are < 5 % for major and < 10% for trace elements. The concentrations of middle REEs and Yb are small. Although XRF counting time was in the range of 300 s/element for each REE, these concentrations should be considered semi-quantitative. Sr and Nd were separated from whole-rock splits using standard chromatographic techniques (for details, see Chen et al. 2002c). Zircons were obtained from the 63 to 125 and 125 to 200 µm sieve fractions by heavy mineral enrichment on a Wilfley table, subsequent magnetic separation on a Frantz isodynamic separator and final density separation using heavy liquids. Whenever possible, grains free of cracks and inclusions were used for analysis. Cathodoluminescence (CL) investigation of zircons similar to those chosen for U–Pb and Pb-evaporation analyses was carried out on a JEOL JXA 8900RL electron microprobe and an LEO 1450 VP scanning electron microscope. For U–Pb isotope analyses, some zircons were air-abraded following the technique of Krogh (1982). The minerals were washed in 6 N HNO_3 and 6 N HCl for half an hour at room temperature and rinsed with ultra-clean H_2O. A mixed $^{205}Pb/^{235}U$ spike was added to the samples before dissolution in a Parr bomb. After dissolution, the solutions were subsequently evaporated, re-dissolved in 0.8 N HBr and passed through minicolumns with a 40-µl bed of AG1-X8 (100–200 mesh) anion exchange resin in a HBr and HCl medium to purify U and Pb. Pb and U were obtained together from the columns, loaded on outgassed Re-filaments together with 0.1 N H_3PO_4 and Si-gel, and run on a Finnigan MAT 262 mass spectrometer. Pb isotopes were measured at ~1,200°C in static mode of collection (Faraday) with ^{204}Pb measured on a secondary-electron multiplier (SEM) in ion-counting mode. Uranium was analysed between 1,300 and 1,350°C using ion counting. Procedure blanks ranged between 5 and 10 pg for Pb and U. Fractionation factors for U and Pb correspond to 0.1% per atomic mass unit. Initial common Pb remaining after

correction for tracer and blank was corrected following the model of Stacey and Kramers (1975). U–Pb data were calculated and plotted with software from Ludwig (1988, 2003).

The technique used for zircon evaporation is that developed by Kober (1986, 1987). Pb isotopes were measured in a mass sequence of 206-207-208-204-206-207 with the SEM. Common lead correction was after Cocherie et al. (1992). Pre-heating of zircon at temperatures of ca. 1,380° serves as a cleaning procedure for micro-inclusions and domains with high common lead component, and therefore, in all analyses the common Pb component was so low ($^{204}Pb/^{206}Pb < 1.3\times10^{-4}$) that calculated ages are largely insensitive to the assumed common Pb composition. The calculated $^{207}Pb/^{206}Pb$ ages are based on the means of all measurements evaluated, and the errors are given by the 2-sigma standard deviation. The age error for a single zircon grain given in Table 2 was calculated according to the formula $\Delta_{age} = \sqrt{(2\sigma/\sqrt{n})^2 + \Delta f^2}$, where n is the number of $^{207}Pb/^{206}Pb$ isotope ratio scans (between 100 and 800 per grain), 2σ is the 2-sigma standard error of the Gaussian distribution function and Δf an assumed uncertainty of the measured $^{207}Pb/^{206}Pb$ ratio of 0.1%, which includes potential bias caused by mass fractionation of Pb isotopes and uncertainty in linearity of the multiplier signal. The amplifiers' non-linearity was tested and found to be < 0.05% in the required counting range (1–500,000 cps). Age and error of several zircons from the same sample are given as weighted mean and error of the weighted mean, respectively. For more details on single zircon Pb-evaporation technique used in this study and standard zircon reproducibility, see Siebel et al. (2003) and Chen et al. (2002a), respectively.

Results

Field observation

Macroscopic and mesoscopic descriptions of palites have been published elsewhere (Troll 1967; Steiner 1969, 1972; Köhler et al. 1989), and here we emphasise on the relationship between host rock and cross-cutting dykes. Field exposures reveal contacts that are generally sharp and lobate (Fig. 2); chilled margins are not observed. In general, the dykes are of variable size and range in width from 1 to 20 m. Individual dykes can be traced in the field for several 100 m along the strike. Compared to the palites, the dykes appear stronger deformed in the field; however, under the microscope quartz deformation and recrystallisation texture can be observed in both rock types. Some dykes have lost their igneous texture and show marked WNW to E-W striking penetrative foliations (e.g. sample 60, Fig. 2f). Along zones where this deformation was intense, the dykes are transformed into mylonites or ultramylonites. These deformation textures can be seen microscopically by grain shape preferred orientation, grain-size reduction and dynamic recrystallisation in pressure shadows of porphyroclasts (Fig. 3). Intrusion relationships between dykes and host rock are best exposed in the Saunstein quarry. One large dyke currently exposed shows increasing deformation textures from the centre towards its northern exposed margin where the rocks are transformed into ultramylonites (Fig. 3d). Shear fabrics seen in the dykes were probably imposed during emplacement as a result of host–rock interaction with a highly viscous silicic melt. It seems likely that the solidifying dykes represent focussed zones of softened material capable of deforming more readily than the massive host rock.

Petrography, geochemistry and Sr–Nd isotopes

A set of nine palites and nine dykes was selected for petrographic and compositional investigation. Geochemistry, isotope composition (four samples) and location of samples are summarised in Table 1, and some of the geochemical results are shown in Fig. 4. Further geochemical data on palites are given in Steiner (1972), Köhler et al. (1989) and Christinas et al. (1991). The palites are observed to contain various proportions of K-feldspar (xeno)megacrysts, plagioclase, biotite, hornblende, interstitial quartz, minor titanite, epidote, pyroxene, apatite and Fe–Ti oxides. In spite of their textural diversity, the chemical compositions mainly correspond to granodiorite, and some analyses plot in the monzonite, monzodiorite and monzogabbro fields (Fig. 4a). With a few exceptions, the rocks are metaluminous [(A/CNK) 0.83–1.06, mainly between 0.9 and 1.0] and highly potassic (K_2O between 3.3 and 7.0 wt%), with a range in SiO_2 contents between 57 and 72 wt%. Chondrite-normalised REE patterns of the palite samples investigated in this study are roughly parallel and these patterns show variable degrees of REE-enrichment and are characterised by a general decrease from La to Yb and a slightly positive to no Eu-anomaly (Fig. 4i).

The mineral composition of the dykes is characterised by the paragenesis quartz, K-feldspar, plagioclase, biotite and ± muscovite. Biotite is often altered to chlorite. All studied dykes contain zircon as U-bearing accessory mineral phase. Dyke compositions include intermediate to felsic varieties. According to the QAP classification (Streckeisen 1976), all samples tightly plot together in the monzogranite field (Fig. 4a) and contain a higher proportion of modal quartz compared to the palites. The studied dykes are moderately peraluminous, [(A/CNK) 1.00–1.17], with SiO_2 contents between 69 and 76 wt%. A marked negative Eu-anomaly can be inferred from the REE spectra for all dykes investigated here (Fig. 4j).

The whole-rock geochemical data reveal a compositional continuum between palites and dykes (Fig. 4). In both rock types, parallel to an increase in SiO_2, there is a decrease of TiO_2, Al_2O_3, Fe_2O_3, MnO, CaO, MgO, P_2O_5, Sr and an increase in Rb, Th, Pb, L(light)REEs and alumina saturation index (A/CNK). The A/CNK

Table 1 Whole-rock compositional data for palites (samples STRO-HB) and granitic dykes (samples FUER-PGD)

Sample	STRO	P1	A159	B85	PF1	GMB	A176b	A111a	HB	FUER	G1	47	G6	G4	FGMH	G5	60	PGD
Easting	4591.98	4601.24	4594.42	4597.19	5390.37	4595.49	4587.37	4593.28	4589.81	4589.35	4592.23	4595.99	4595.34	4595.45	4591.40	4594.88	4597.86	5390.37
Northing	5416.32	5414.03	5415.74	5410.37	5407.15	5415.66	5417.03	5416.65	5417.85	5415.83	5414.35	5413.33	5414.53	5414.07	5414.13	5413.56	5413.86	5407.15
SiO_2	57.3	58.7	59.1	60.2	62.1	67.5	67.6	67.8	71.9	69.1	71.0	72.0	72.4	72.5	73.2	74.1	75.7	75.9
TiO_2	0.80	1.06	1.53	0.87	0.78	0.47	0.63	1.10	0.34	0.72	0.37	0.31	0.29	0.26	0.23	0.19	0.10	0.13
Al_2O_3	17.2	18.2	16.0	18.4	16.5	16.3	15.4	15.1	15.2	14.0	14.2	13.0	12.9	13.1	14.8	12.6	13.0	12.9
Fe_2O_3	6.23	5.46	7.05	4.15	4.57	2.4	3.13	2.96	1.79	3.22	2.02	1.49	2.38	1.55	1.48	1.80	1.04	0.99
MnO	0.10	0.05	0.10	0.06	0.07	0.02	0.04	0.03	0.02	0.05	0.02	0.02	0.02	0.02	0.02	0.03	0.04	0.02
MgO	3.30	2.75	2.54	1.92	2.38	1.23	1.70	0.89	0.93	0.64	0.54	0.27	0.31	0.38	0.40	0.22	0.17	0.10
CaO	3.36	4.61	4.09	3.77	3.56	3.23	2.69	1.96	1.49	1.19	0.84	0.93	0.57	0.77	0.72	0.49	0.64	0.89
Na_2O	2.89	3.97	3.36	3.74	3.34	4.27	3.44	3.03	2.46	2.93	2.97	2.88	2.68	3.11	3.34	2.87	3.39	3.62
K_2O	5.99	3.97	4.03	5.17	4.41	3.34	4.41	5.87	7.00	5.73	5.67	5.99	5.87	5.62	5.37	5.79	5.11	4.47
P_2O_5	0.58	0.47	0.68	0.32	0.32	0.18	0.19	0.28	0.21	0.28	0.29	0.05	0.06	0.19	0.32	0.06	0.03	0.02
Total	97.7	99.2	98.5	98.6	98.0	98.9	99.3	99.0	99.2	97.8	97.9	97.0	97.5	98.3	99.8	98.1	99.2	99.1
Ba	3430	1108	1362	3327	1107	922	1244	2716	2568	897	389	337	376	291	277	236	78	9
Rb	179	187	142	149	158	84	157	122	179	269	355	344	386	352	231	411	520	340
Sr	519	567	531	1163	456	571	486	676	619	110	90	86	88	77	62	67	58	31
Y	28	29	63	18	21	12	16	37	15	55	17	28	27	20	13	33	48	23
Zr	137	473	625	382	361	170	220	875	154	482	179	176	183	141	74	149	117	99
Pb	31	23	24	29	32	25	30	34	31	36	32	35	40	33	31	32	43	35
Th	5.5	8.2	17	17	5.9	8.2	7.8	15	8.4	34	45	54	53	31	14	47	33	56
La	40	43	106	38	34	41	30	41	37	80	68	84	73	60	23	62	38	50
Ce	84	90	224	92	76	57	54	60	48	165	104	174	151	72	37	118	63	75
Nd	40	53	125	42	37	31	26	30	28	80	58	76	62	32	24	49	37	31
Sm	5.1	7.0	15	4.9	4.7	2.3	2.7	3.2	3.3	11	11	11	10	5.8	2.6	5.3	6.3	7.3
Eu	1.4	1.2	2.2	2.6	1.2	1.3	1.1	1.5	1.4	0.9	0.7	0.7	0.6	0.2	0.1	0.1	0.1	0.3
Yb	2.7	2.1	5.1	1.1	1.5	0.7	1.0	1.9	1.1	4.5	1.4	2.3	2.5	1.8	1.0	3.1	4.8	2.2
$\sum$ LREE	169	193	470	152	177	131	113	134	116	336	241	345	296	170	234	144	87	163
A/CNK	0.99	0.95	0.93	0.99	0.97	0.98	1.01	1.01	1.06	1.06	1.13	1.00	1.10	1.10	1.17	1.06	1.06	1.04
$^{87}Sr/^{86}Sr_i^a$	–	0.70772	–	–	0.70789	–	–	–	–	–	0.71177	–	–	–	–	–	–	0.71467
ϵNd_i^a	–	−4.2	–	–	−4.6	–	–	–	–	–	−6.5	–	–	–	–	–	–	−4.3

– not determined

Major elements in wt%, trace elements in ppm

A/CNK alumina saturation index: mol%[Al_2O_3/($CaO + Na_2O + K_2O$)]

[a]Initial $^{87}Sr/^{86}Sr$ ratios and ϵNd values calculated for $T = 330$ Ma (uncertainties of measured ratios were ±1% for $^{87}Rb/^{86}Sr$, ±0.003% for $^{87}Sr/^{86}Sr$ and ±0.3 for ϵNd value)

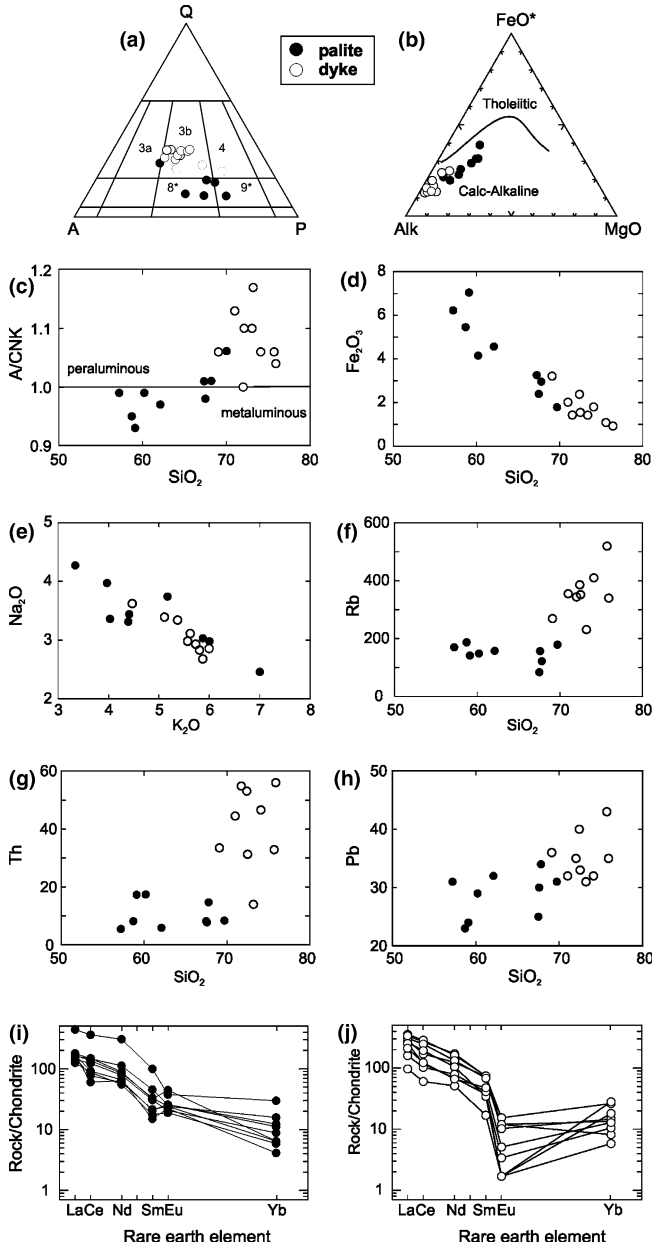

Fig. 4 Geochemical classification and selected major- and trace-element diagrams illustrating the geochemical composition of host rocks (*filled circles*) and cross-cutting dykes (*open circles*); **a** Samples in the QAP diagram; fields based on Streckeisen (1976): *3a* syenogranite, *3b* monzogranite, *4* granodiorite, *8** quartz monzonite, *9** quartz monzodiorite, **b** AFM ternary plot with tholeiitic and calc-alkaline division showing that the palites and cross-cutting dykes share a calc-alkaline trend, **c** A/CNK versus SiO_2, horizontal line shows the boundary between metaluminous and peraluminous rocks, **d** Fe_2O_3 versus SiO_2 diagram; similar trends can be found for other major elements such as TiO_2, Al_2O_3, MnO, CaO, MgO and P_2O_5 (not shown), **e** K_2O versus Na_2O; **f–h** Rb, Th and Pb versus SiO_2, **i** and **j** Chondrite normalised REE diagrams for palites and dykes, respectively. Chondrite concentrations of McDonough and Sun (1995) were used for REE normalisation.

versus SiO_2 correlation trend crosscuts the metaluminous/peraluminous boundary (Fig. 4c). Na_2O and K_2O show a negative correlation and vary more in the palites than in the cross-cutting dykes, but there is no systematic difference in concentration of these elements in both rock types (Fig. 4e). Sr and Nd isotope compositions were determined for two dykes and two host rocks (Table 1). Measured ratios were corrected for in-situ decay with an age of 330 Ma (based on age results outlined below). Initial $^{87}Sr/^{86}Sr$ ratios are higher in the dykes (0.7118 and 0.7147) than in the host rocks (0.7079 and 0.7077), whereas initial ϵNd-values are at −6.5 and −4.3 in two dykes and at −4.3 and −4.6 in two host rocks.

U–Pb and Pb–Pb zircon geochronology

Analyses were performed using the U–Pb method on single grains, broken pyramidal ends of larger grains or multi-grain fractions (maximum up to four small grains) and the Pb-evaporation method on single zircon grains. Pb-evaporation data are listed in Table 2 and U–Pb analytical data are given in Table 3. CL studies were performed to evaluate the macrostructural characteristics, and representative images (Fig. 5) are discussed together with the geochronological data.

Palites

The two samples selected for dating (PF1 and P1) contain large, elongated, long- to short-prismatic, colourless idiomorphic zircons with some dark inclusions (Fig. 6a), and CL investigations show the homogeneous "interior", i.e. microstructural homogeneity of these zircons (Fig. 5, zircons A1–A5 and B1–B5). The grains exhibit oscillatory zoning, i.e. banding of CL dark and CL light regions, and some exhibit different growth stages (Fig. 5, grains A2 and A3) but are generally free of inherited cores. Zircons chosen for dating were the most transparent and least-cracked grains from each sample.

Measurements employing the single grain Pb-evaporation method by different evaporation steps lead to $^{207}Pb/^{206}Pb$-ages of zircons from sample P1 between 332 and 338 Ma with a mean age of 334 ± 3 Ma (Fig. 7, Table 2). Six zircon grains from sample PF1 yielded Pb-evaporation ages between 333 and 336 Ma with a mean age of 334.5 ± 1.1 Ma. From sample PF1, nine zircon fractions were analysed by U–Pb isotope dilution method. They plot along the concordia and define $^{206}Pb/^{238}U$ ages between 327 and 342 Ma and $^{207}Pb/^{235}U$ ages between 329 and 341 Ma (Fig. 8a) with data spread slightly too large for a single-phase zircon population.

Zircons from samples PF1 and P1 possess similar calculated Th/U ratios between 0.26 and 0.51 (calculated from $^{208}Pb/^{206}Pb$ ratios and age of sample). Variation of this ratio, that is generally thought to reflect spatial variation of the Th/U ratio within the zircon crystal (Klötzli 1999), becomes evident from the evaporation data (Fig. 7). Zircons from sample PF1 show increasing

Table 2 Data from zircon $^{207}Pb/^{206}Pb$ evaporation analyses (palite samples P1 and PF1)

Sample	No. of ratios	$^{204}Pb/^{206}Pb$	$^{206}Pb/^{208}Pb$	Th/U[a]	$^{207}Pb/^{206}Pb$	$^{207}Pb/^{206}Pb$ age (Ma)
P1-1	484	0.000032	9.4	0.33	0.053106 ± 22	333.4 ± 2.5
P1-2	292	0.000129	12.4	0.26	0.053084 ± 46	332.4 ± 3.0
P1-3	717	0.000085	7.0	0.45	0.053079 ± 20	332.2 ± 2.5
P1-4	322	0.000040	11.9	0.27	0.053117 ± 46	333.8 ± 3.0
P1-5	446	0.000044	10.3	0.31	0.053214 ± 26	338.0 ± 2.6
Weighted average						334.0 ± 3.0
PF1-1	555	0.000057	10.4	0.30	0.053137 ± 42	334.7 ± 2.9
PF1-2	554	0.000131	11.0	0.36	0.053140 ± 38	334.8 ± 2.8
PF1-3	367	0.000021	7.6	0.43	0.053117 ± 63	333.8 ± 3.5
PF1-4	593	0.000032	12.6	0.26	0.053163 ± 22	335.8 ± 2.5
PF1-5	625	0.000035	12.5	0.26	0.053104 ± 45	333.3 ± 3.0
PF1-6	331	0.000101	10.1	0.31	0.053121 ± 37	334.0 ± 2.8
Weighted average						334.5 ± 1.1

[a]Th/U model ratio calculated from $^{208}Pb/^{206}Pb$ ratio and age of the sample

$^{208}Pb/^{206}Pb$ ratios with increasing evaporation temperature. $^{208}Pb/^{206}Pb$ ratios in zircons from numerous granitoids in NE Bavaria vary in the same way (Siebel et al. 2003) indicating that the Th/U ratio has decreased during magmatic growth from the inner to the outer sector of the crystal. Zircons from sample P1 either show no clear trend or a decrease of $^{208}Pb/^{206}Pb$ ratios with increasing evaporation temperature (Fig. 7). It is likely that the Th/U chemical zoning varies according to the coexisting mineral assemblage present during crystallisation and largely depends on the presence or absence of concurrent growth or co-precipitation of other Th-bearing phases such as allanite or monazite.

Granitic dykes

Zircons from all four investigated dyke samples display concentric magmatic zoning and apart from few grains (grains C5 and E3 in Fig. 5) show no clear evidence for the presence of inherited cores. Sample *PGD* contains small red zircon crystals (Fig. 6b) that show no CL emission at all. CL intensity in zircons depends on structural parameters such as crystallinity (Nasdala et al. 2002) and on trace element abundances, and emission is inversely correlated to their contents of U and Y (e.g. Hanchar and Miller 1993; Kempe et al. 2000). In sample PGD, the U content is anomalously high (between 3,000–25,000 ppm) and might be the main reason for the suppressed CL signal of zircons from this sample. Calculated Th/U ratios of zircons from sample PGD mainly vary between 0.19 and 0.54 and are indicative for zircon formed from igneous crystallisation (Rubatto and Gebauer 2000). Fraction PGD-9a yields an outstanding high Th/U ratio of 32 and high Pb concentration (1,340 ppm), that is probably caused by a Th-mineral inclusion. The mechanically untreated (non-abraded) zircons suffered variable Pb loss, resulting in a dispersion of apparent $^{206}Pb/^{238}U$ and $^{207}Pb/^{235}U$ ages between 321 and 254 Ma (4.1–18.6% discordant). Six zircon fractions (PGD-7a to PGD-12a in Table 3) were air-abraded (Krogh 1982) before analysis and approximately 10–20% of the entire volume of each zircon was removed by this procedure. Air-abrasion did not minimise the degree of discordance and four fractions still give discordant (1.1–18.8%) results (Fig. 8b). However, two of these abraded fractions plot on the concordia close to 320 Ma. All fractions (abraded and non-abraded) plot on a discordia line that gives an upper intercept age of 322 ± 5 Ma (MSWD = 3.1, all errors for discordia intercepts refer to 95% confidence limit). The lower intercept indicates that the main Pb-loss event seems to have occurred in more recent times.

The zircon population recovered from the leucocratic dyke *60* (Fig. 2b) includes elongated prismatic grains that appear hazy, ranging in colour from honey-yellow through brown to red. The CL images display oscillatory zoning supporting their magmatic origin (Fig. 5, grains C1–C5). Two fractions plot on the concordia curve at 329 and at 324 Ma (Fig. 8c), whereas the remaining three fractions plot slightly below the concordia (2.3–5.5% discordance) indicating some Pb-loss. A discordia line through all fractions yields an upper intercept age of 326 ± 9 Ma (MSWD = 1.9). The U content of the grains ranges from 379 to 1808 ppm, i.e. lower than in PGD, and the calculated Th/U ratios vary between 0.37 and 0.75.

Dyke sample *G1* contains a high percentage of clear or colourless long-prismatic grains with aspect ratios > 4. The majority of the zircon crystals are euhedral with simple prismatic-pyramidal morphology and show a remarkable variation in size (~40–300 μm). CL images show that the zircon grains exhibit zoned texture (Fig. 5, D1–D5). The U–Pb results of nine fractions are shown in Fig. 8d. Most data points plot on the concordia curve and comprise fractions around 326, 322 and 315–318 Ma. An additional fraction lies discordant at ca. 290 Ma. Two data points plot on the concordia at 339 Ma substantiating an older component in the dyke. All data points define a discordia yielding an upper intercept age of 331 ± 8 Ma (MSWD = 1.1). All fractions have intermediate to high U contents (435–1760 ppm) and calculated Th/U ratios vary between 0.11 and 0.96.

Table 3 Data from zircon U–Pb isotope dilution analyses

Sample/Fraction[a]	Weight[b](mg)	$^{206}Pb/^{204}Pb$[c]	U[b] (ppm)	Pb[b] (ppm)	Th/U[d]	Isotopic ratios[e]			Calculated ages (Ma)			Percentage of discordance[f]
						$^{206}Pb/^{238}U$	$^{207}Pb/^{235}U$	$^{207}Pb/^{206}Pb$	$^{206}Pb/^{238}U$	$^{207}Pb/^{235}U$	$^{207}Pb/^{206}Pb$	
PF1-1	0.031	1905	699	37	0.33	0.05251 ± 33	0.3844 ± 24	0.053098 ± 38	330	330	333	0.9
PF1-2	0.020	681	515	30	0.51	0.05303 ± 60	0.3885 ± 49	0.05314 ± 28	333	333	335	0.6
PF1-3	0.031	2075	555	29	0.35	0.05214 ± 59	0.3809 ± 45	0.05298 ± 17	328	328	329	0.1
PF1-4	0.025	939	321	17	0.41	0.05211 ± 31	0.3822 ± 28	0.05320 ± 22	327	329	337	2.9
PF1-5	0.080	8347	381	21	0.39	0.05318 ± 27	0.3904 ± 21	0.053250 ± 88	334	335	339	1.5
PF1-6	0.099	7752	418	22	0.36	0.05259 ± 27	0.3853 ± 22	0.05313 ± 13	330	331	335	1.4
PF1-7	0.040	6612	399	21	0.30	0.05259 ± 28	0.3848 ± 24	0.05307 ± 17	330	331	332	0.5
PF1-8	0.177	552	355	21	0.51	0.05410 ± 28	0.3977 ± 25	0.05332 ± 18	340	340	342	0.7
PF1-9	0.108	3052	404	23	0.40	0.05441 ± 37	0.3987 ± 28	0.053147 ± 63	342	341	335	-2.0
PGD-1	0.090	11643	5139	238	0.22	0.04786 ± 28	0.3476 ± 21	0.052667 ± 18	301	303	314	4.1
PGD-2	0.080	13441	3690	175	0.34	0.04750 ± 83	0.3455 ± 60	0.052749 ± 19	299	301	318	6.1
PGD-3	0.080	13909	3615	160	0.36	0.04391 ± 23	0.3196 ± 17	0.052784 ± 20	277	282	320	13.7
PGD-4	0.044	3780	10630	424	0.29	0.04026 ± 29	0.2919 ± 21	0.052586 ± 23	254	260	311	18.6
PGD-5	0.023	6136	13936	627	0.19	0.04679 ± 27	0.3406 ± 20	0.052784 ± 20	295	298	320	8.1
PGD-6	0.045	5186	5767	261	0.24	0.04633 ± 45	0.3371 ± 33	0.052775 ± 24	292	295	319	8.7
PGD-7*a*	0.005	106	4784	330	1.32	0.04103 ± 23	0.2985 ± 31	0.05275 ± 44	259	265	318	18.8
PGD-8*a*	0.005	2250	4676	254	0.54	0.05098 ± 27	0.3718 ± 21	0.05289 ± 13	321	321	324	1.1
PGD-9*a*	0.016	1332	3161	1340	32	0.04316 ± 40	0.3125 ± 30	0.05251 ± 10	272	276	308	11.8
PGD-10*a*	0.005	5377	20205	919	0.28	0.04609 ± 28	0.3346 ± 21	0.052655 ± 37	291	293	314	7.7
PGD-11*a*	0.010	2132	21234	976	0.27	0.04627 ± 24	0.3362 ± 18	0.052699 ± 28	292	294	316	7.9
PGD-12*a*	0.006	8549	24786	1213	0.22	0.05061 ± 26	0.3689 ± 19	0.052868 ± 26	318	319	323	1.5
60–1	0.067	3211	1808	89	0.37	0.04870 ± 47	0.3552 ± 34	0.052897 ± 51	307	309	324	5.5
60–3	0.040	2598	604	32	0.40	0.05238 ± 27	0.3828 ± 21	0.053005 ± 70	329	329	329	0.0
60–4	0.040	2499	492	25	0.44	0.04911 ± 26	0.3578 ± 22	0.05284 ± 15	309	311	322	4.1
60–5	0.035	2412	379	22	0.75	0.05160 ± 49	0.3761 ± 37	0.05288 ± 13	324	324	323	−0.4
60–6	0.030	2923	807	41	0.39	0.04990 ± 44	0.3634 ± 33	0.05282 ± 12	314	315	321	2.3
G1-1	0.021	1121	435	24	0.32	0.05393 ± 31	0.3959 ± 33	0.05323 ± 31	339	339	339	0.1
G1-2	0.012	430	534	32	0.46	0.05395 ± 30	0.3953 ± 41	0.05314 ± 44	339	338	335	−1.1
G1-3	0.011	2003	776	38	0.22	0.05032 ± 27	0.3670 ± 33	0.05290 ± 36	316	317	325	2.7
G1-4	0.007	1220	664	33	0.24	0.05008 ± 31	0.3645 ± 49	0.05280 ± 61	315	316	320	1.6
G1-5	0.022	7412	1440	69	0.11	0.05120 ± 28	0.3735 ± 22	0.052910 ± 95	322	322	325	1.0
G1-6	0.016	2928	741	36	0.24	0.05026 ± 27	0.3687 ± 27	0.05320 ± 26	316	319	337	6.3
G1-7	0.008	620	813	46	0.55	0.05205 ± 38	0.3790 ± 71	0.05281 ± 87	327	326	321	−2.2
G1-8	0.005	626	1760	84	0.36	0.04563 ± 28	0.3303 ± 35	0.05251 ± 44	288	290	308	6.6
G1-9	0.002	168	1008	67	0.96	0.05064 ± 69	0.366 ± 20	0.0524 ± 26	318	317	304	−5.2
G4-1	0.014	1278	962	51	0.25	0.05315 ± 33	0.3888 ± 29	0.05305 ± 21	334	334	331	−0.9
G4-2	0.005	152	218	18	1.50	0.05184 ± 32	0.3817 ± 37	0.05341 ± 38	326	328	346	6.0
G4-3	0.099	727	844	44	0.47	0.04829 ± 27	0.3524 ± 33	0.05293 ± 38	304	307	326	6.9
G4-4	0.010	870	1034	49	0.24	0.04701 ± 27	0.3444 ± 29	0.05314 ± 31	296	301	335	11.9
G4-5	0.004	457	1595	99	1.16	0.04817 ± 28	0.3521 ± 38	0.05302 ± 47	303	306	330	8.3
G4-6	0.009	409	1551	101	0.92	0.05267 ± 28	0.3818 ± 28	0.05258 ± 26	331	328	311	−6.5

PF1 palite, all other samples are dykes

[a]All zircon fractions; *a* air-abraded fraction (Krogh 1982)

[b]Weight and concentration error better than 20%

[c]Measured ratio corrected for mass discrimination and isotope tracer contribution

[d]Th/U model ratio calculated from $^{208}Pb/^{206}Pb$ ratio and age of the sample

[e]Corrected for blank Pb, U and initial common Pb based on the Stacey and Kramers (1975) model; errors are $2\sigma_m$

[f]Degree of discordance (%) for the given $^{207}Pb/^{206}Pb$ age of the fraction

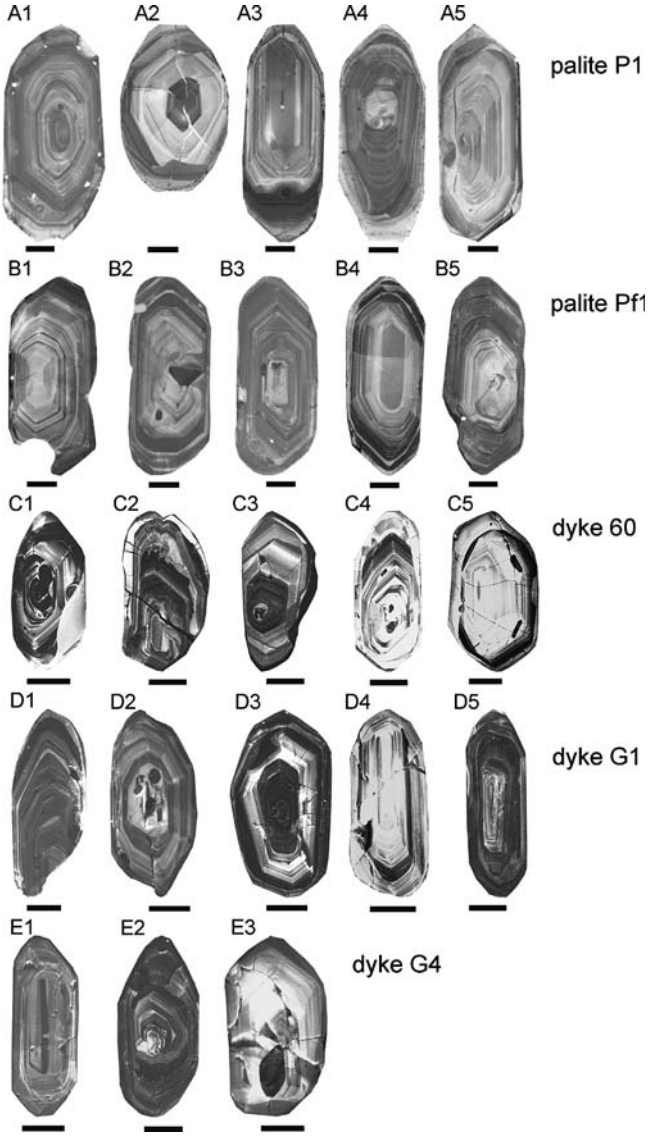

Fig. 5 Cathodoluminescence images of polished zircon sections from host rocks and cross-cutting dykes. Grains from both rock types show oscillatory zoning with alternating bands of bright and dark luminescence intensities mainly parallel to the growing crystal faces. *A1–A5* and *B1–B5* internal structure of characteristic zircons from the palite samples P1 and PF1, *C1–C5* typical zircons from dyke 60, *D1–D5* typical zircon from dyke sample G1, *E1–E5* typical zircons from dyke G4. Note that in zircons from dyke sample PGD (not shown), CL is suppressed probably by high U abundance. Images for palites were obtained with a Jeol JXA 8900RL electron microprobe and those for dykes with a Leo Scanning Electron Microscope. The more brightly luminescent domains of dyke zircons compared to host rock may be due to different microscopic techniques. Scale bars are 30 μm

The zircon population extracted from dyke *G4* exhibits a variety of forms including well-preserved euhedral to subhedral transparent to translucent crystals of various size and equant to needle-like shape. CL images show no significant internal features apart from oscillatory zoning typical for magmatic zircons (Fig. 5, E1–E3). The U–Pb data define two distinct groupings (Fig. 8e). Three data points plot close to the concordia

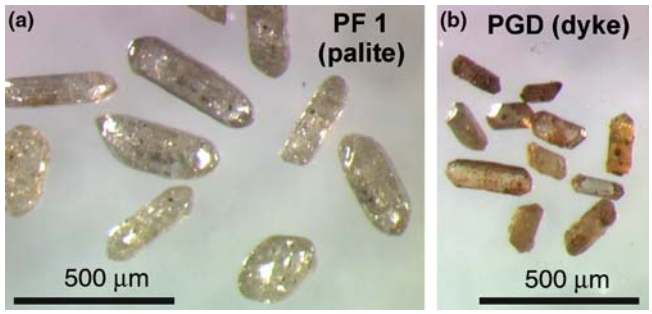

Fig. 6 Photomicrographs of zircons from **a** host rock PF1, **b** cross-cutting dyke PGD (for outcrop locality see Fig. 2a). The *dark red spots* within the zircons from the dyke come from impurities and small inclusions. Zircons from this sample are "leaky" with respect to Pb and up to 20% discordant

at 330 Ma and one of them is slightly reversely discordant. The second group of points are discordant. When these analyses are regressed by forcing through zero (i.e. present day), an upper intercept age of 331 ± 9 Ma (MSWD = 0.37), that coincides with the average age of the older fractions, is obtained. All zircon fractions of this sample have intermediate to high U contents (218–1595 ppm) and intermediate to high Th/U ratios of 0.24–1.50.

Relationship between Th/U ratio, $^{206}Pb/^{238}U$ age and U content for all investigated zircon fractions is compiled in Fig. 9. Whereas U-poor fractions show a large range in Th/U ratios, the U-rich fractions are mainly characterised by low Th/U ratios (Fig. 9a). However, it is interesting to note that the Th/U ratio does not continue to decrease in the extreme U-rich fractions (i.e. > 3,000 ppm U), implying that most of the U-rich fractions are also rich in Th. This would not be expected if the zircon were affected by later fluid infiltrations due to the higher mobility of U compared to Th. Most calculated Th/U ratios are in the range typical for magmatic zircons and higher than in metamorphic zircons (Rubatto and Gebauer 2000; Rubatto 2002). The relationship between the U content and apparent U–Pb ages will be discussed in the following section.

Discussion

Age constraints on host rock

Based on the data presented here, the age of the palites is confined to the Lower Carboniferous. U–Pb and Pb–Pb-evaporation analyses yield ages of 334 ± 3 and 334.5 ± 1.1 Ma (average $^{207}Pb/^{206}Pb$-evaporation zircon ages of samples P1 and PF1, respectively) and 327–342 and 328–341 Ma (range of $^{206}Pb/^{238}U$ and $^{207}Pb/^{235}U$ ages of sample PF1). These ages are some 140 Ma younger than the Ordovician Rb–Sr isochron age obtained from different whole-rock samples (Christinas et al. 1991). Although in recent years Ordovician magmatism was confirmed by SHRIMP zircon analyses in

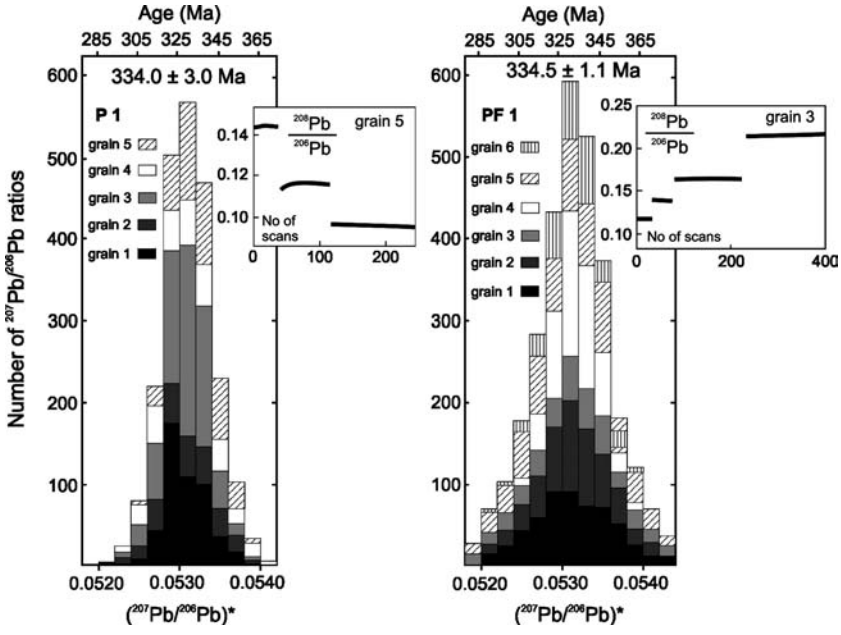

Fig. 7 Histograms showing the distribution of radiogenic $^{207}Pb/^{206}Pb$ ratios obtained from evaporation analyses of zircons from the palite samples P1 (*left*) and PF1 (*right*). *Insets* show the $^{208}Pb/^{206}Pb$ distribution obtained from different evaporation steps for a given zircon grain

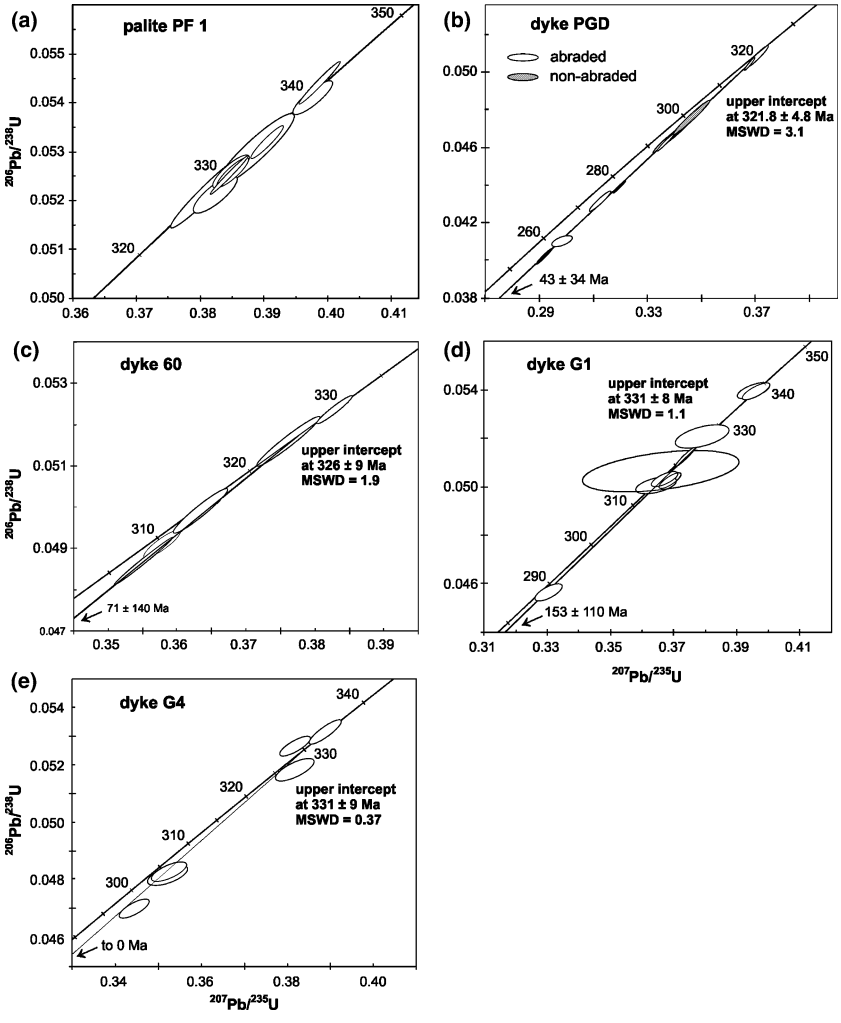

Fig. 8 Concordia diagrams showing U–Pb data for zircons from a host rock and four different dykes. For the dykes, discordia lines generated by variable Pb loss of the U-rich zircon fractions are added to the figure; **a** Palite PF1 (host rock) with nine concordant or nearly concordant fractions, **b** dyke PGD, different shading of ellipses to distinguish abraded (*white*) and non-abraded (*dark*) zircon fractions, **c** dyke 60, **d** dyke G1, **e** dyke G4. *Ellipses* indicate the uncertainty at the 2σ level (95% confidence level)

different regions of the SW Moldanubian zone (Mielke et al. 1996; Teipel et al. 2003), the new data for the palites exclude an Ordovician formation and the Rb–Sr age therefore most likely represents a mixing line (comp. Holl et al. 1989). In all analysed grains, no clear evidence of inheritance or Pb-loss was found. The excess scatter

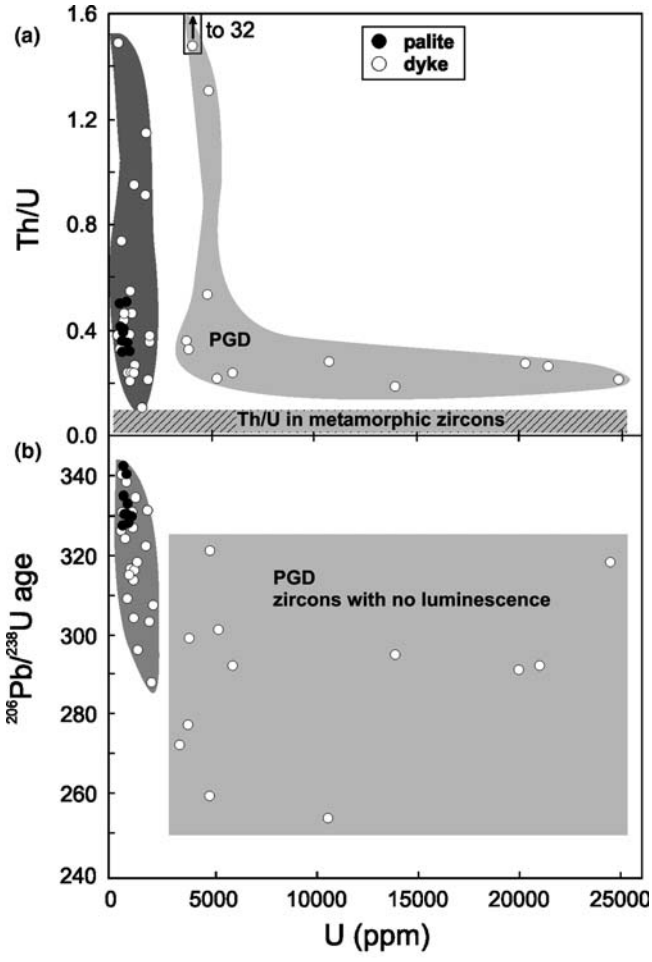

Fig. 9 Plots showing the Th/U ratio, $^{206}Pb/^{238}U$ age and U content of the zircon fractions of host rock and cross-cutting dykes; **a** Th/U (calculated from the Pb isotope data) versus U concentration (in ppm) diagram. *Inset with arrow* indicates fraction with a calculated Th/U ratio of 32 (PGD-*9a*), **b** $^{206}Pb/^{238}U$ ages as a function of U content. Analyses within the *dark shaded field* show negative correlation between apparent ages and U concentration, indicating Pb loss controlled by radiation damage. In both figures, *bright shaded field* comprises non-luminescent fractions from sample PGD with U content > 3,000 ppm

of concordant $^{206}Pb/^{238}U$ and $^{207}Pb/^{235}U$ ages in sample PF1, however, might indicate mixing of two episodes of zircon growth (i.e. ~340 and ~330 Ma) which would fit with the core-rim relationships visible in grains A2, A3 and A5 (Fig. 5). Sample PF1 was taken in close proximity to dyke PGD. The first episode of zircon growth may be related to the crystallisation from the palite melt and the second could be to thermal or hydrothermal influence during dyke emplacement.

The U–Pb and Pb–Pb ages confirm previous suppositions from field observations (e.g. Troll 1967) that the palites are of late-Variscan age. The deformation textures suggest that these rocks were formed during high-temperature shearing. As known from other crustal-scale shear zones, e.g. Red River, Yunnan (Zhang and Schärer 1999) and Ivrea-Verbano, Alps (Mulch et al. 2002), magmatic activity often occurs in direct relation to strike-slip movement. Therefore, it seems likely, that there was a link between formation of the palites and deformation related to the Pfahl zone. This means that the Pfahl shear zone was already active during the Lower Carboniferous.

For other late-Variscan granitoids in the Bavarian Forest close to the Pfahl zone, slightly younger U–Pb zircon and monazite ages were reported (Kristallgranit I, ~315 Ma, Grauert et al. 1974; Propach et al. 2000; Ödwieser granodiorite, 318 and 320 Ma, Propach et al. 2000). Compared to the palites, these magmatic rocks are hardly affected by late-Variscan deformation and are probably not related to the initiation of the Pfahl zone. A regional comparison with rocks outside the Pfahl zone shows that the age of the palites is indistinguishable from that of the Fürstenstein diorites (~335 Ma, Chen et al. 2002b) and the Rastenberg granodiorite, Upper Austria (338 ± 2 Ma, Klötzli and Parrish 1996). The age is also in the range of U–Pb zircon ages obtained from granitoids of the Central Bohemian Batholith (330–350 Ma, e.g. Franke 2000; Janoušek and Gerdes 2003) and correlates with metamorphic monazite ages in the Austrian and Czech parts of the Drosendorf assemblage (Friedl et al. 1993, 1993; Gebauer and Friedl 1994, see also Franke 2000).

Age constraints on dykes

Three out of four investigated dykes contain some zircon fractions that nearly approach the age of the host rock. Most fractions, however, plot in a slightly discordant manner or yield younger concordant ages. Dyke sample G1 contains two zircon fractions with U–Pb ages of ~339 Ma. It seems rather unlikely that these ages represent the dykes' emplacement time. More likely, these zircons might have grown during an earlier igneous crystallisation event. During melting, they might have been incorporated in the magma and they now form complete xenocrysts in the dykes. Alternatively, these fractions might comprise accidental grains incorporated from host-rock xenoliths during emplacement.

In contrast to the zircons from the palites, the dyke zircons plot up to 20% below concordia (Fig. 8). Most of the dyke zircons contain much higher U concentration compared to those of the palites (Fig. 9b) and this is the most likely reason for the different behaviour. Compared to zircons with low U concentration, zircons enriched in U might be expected to be more susceptible to Pb-loss due to accumulated radiation damage of the crystal lattice caused by α-particles and fission products (Silver and Deutsch 1963; Woodhead et al. 1991; Mezger and Krogstad 1997). Such metamict zircons often show differential rejuvenation, i.e. an increase in discordance. Excluding some fractions with the highest U content (PGD), there is a slight negative correlation between the apparent $^{206}Pb/^{238}U$ age and the U concentration, i.e. grains with higher U concentration yield younger ages (Fig. 9b). Although trace element content in zircons can

vary largely (Hinton and Upton 1991; Rubatto 2002) such high U concentrations, as found in zircons of sample PGD, are strongly indicative of the presence of some U (and Th) within inclusions (Gorz 1974), a possible explanation for the lack of a clear correlation between apparent age and U concentration in fractions from sample PGD.

If a later Pb-loss event for the dyke zircons is assumed, the time of dyke emplacement can be inferred from the upper discordia intercepts at about 322 ± 5 Ma (sample PGD), 326 ± 9 Ma (sample 60), 331 ± 8 Ma (sample G1) and 331 ± 9 Ma (sample G4) (Fig. 8b–e). A certain degree of inconfidence must be attributed to the slightly younger age of sample PGD based on the probability of nearly complete, non-recent Pb-loss. Due to their extremely high U concentration, zircons from sample PGD are definitely affected by metamictisation and might have already become severely metamict a few Ma after formation. The natural annealing of metamict zones does take place only above the amorphisation temperature and severely metamict zircons may therefore lose their Pb at low temperature conditions (Cherniak et al. 1991; Meldrum et al. 1998; Cherniak and Watson 2000). Pb can also be readily leached from metamict zircons under hydrothermal conditions (e.g. Pidgeon et al. 1966; Sinha et al. 1992). Thus, zircons from sample PGD could become susceptible to Pb loss either during or after late-Variscan regional high-temperature metamorphism (326–322 Ma, Kalt et al. 2000), or when hydrothermal fluids circulated through the Pfahl zone. It is therefore likely that the upper intercept age of sample PGD only provides an approximation of the minimum age of this dyke. In sample G1, several fractions which are analytically concordant plot between 315 and 320 Ma (Fig. 8d); the coincidence in age of several fractions may likewise result from near-complete resetting shortly after emplacement. Given the coincidence (within error) between the upper intercept ages of samples 60, G1 and G4, we believe that these ages represent a close approximation for the time of zircon growth. Combining all observations, we suggest that dyke intrusion took place shortly after palite formation at around 330 Ma. Compared to the palites and dykes analysed in this study, other granitoids adjacent to the Bavarian Pfahl zone (Patersdorf granite and Rinchnach granite) are largely undeformed. The emplacement ages of these post-tectonic granitoids still have to be determined in order to define the lower age limit of the penetrative mylonitisation event in the Bavarian shear zone.

Significance of compositional variation

Nearly all dykes were found within the palite zone which raises the possibility of a genetic relationship between both rock types. The continuous chemical variation between palites and cross-cutting dykes (Fig. 4) could result from various processes including magma mixing or fractional crystallisation. Palites and dykes have several geochemical features in common such as similar range of Na_2O and K_2O; compositional variation (i.e. increase of SiO_2 from palites to dykes combined with linear decrease of Ti, Al, Fe, Mn, Ca, Mg, P and Sr) suggests that both rock types could have formed through fractional crystallisation of the same parental magma. Compared to the palites, the dykes show a significant negative Eu-anomaly, which is a reflection of a larger amount of feldspar fractionation (Nagasawa and Schnetzler 1971). Despite these relationships, the dykes are generally more enriched in LREE than the palites (Table 1). Such a feature is not consistent with a model of in-situ fractional crystallisation because increasing differentiation of a granitic melt decreases the LREE due to fractionation of trace phases such as allanite or monazite (e.g. Miller and Mittlefehldt 1982; Michael 1984). High LREE content in the dykes can be attributed to the suspension of allanite or monazite fractionation in the parental melt. Th is a major element in both monazite and allanite, and the high Th content observed in the dykes (Fig. 4g) probably reflects the presence of one of these minerals. We argue that the dykes were derived from a fractionated metaluminous parental melt that was enriched in LREE and Th. Enrichment of LREE can be achieved in a more mafic magma before attainment of allanite saturation. Generally, the LREE rich accessory phase in a metaluminous melt is allanite. Thus, we think that the dykes were derived from a mafic parental magma that has fractionated apatite and or epidote instead of allanite, producing a final melt enriched in LREE and Th.

The isotope data reveal evidence of considerable variation of the initial $^{87}Sr/^{86}Sr$ isotope ratios between host rock and dykes. Including an initial $^{87}Sr/^{86}Sr$ ratio of 0.7358 ± 0.0001 (dyke sample studied by Christinas et al. 1991), it becomes evident that the dykes are likely to have been affected by Sr isotopic disturbances. Subsolidus hydrothermal alteration has a great potential to redistribute the Sr isotopic composition, and the addition of Rb from circulating solutions would also result in enhanced initial Sr ratios (Siebel 1995). Given the low mobility of the REE, the Nd isotope ratios can provide a better image of the source. Dyke PGD has almost the same ϵNd_i (−4.3) as the two palite samples (−4.2 and −4.6), indicating that these rocks could have been derived from the same source. However, the difference between the Nd isotope composition of dyke G1 ($\epsilon Nd_i = -6.5$) and the palites may indicate the involvement of crustal contamination during the formation of this dyke. Given the limited number of isotope data, it remains somewhat enigmatic to which extent palites and dykes were derived from related sources.

The absence of muscovite, cordierite and Al-silicates (except in local retrograde zones) indicates that the palites cannot be regarded as a product of in-situ partial melting of the adjacent gneisses (Perlgneise) south of the Pfahl zone. Besides, the palites have higher Nd values compared to common Moldanubian gneisses (Liew and Hofmann 1988), indicating a different source. The gen-

eral lack of inherited zircon components is compatible with melting of the lower crust at very high temperatures or with direct contribution of a mafic mantle melt as already proposed by Christinas et al. (1991). In addition, the frequency of metabasic inclusions in the palites argues against a derivation purely by crustal anatexis and implies that some of the melts have formed in the mantle. Due to shear zone activity, these melts could have migrated through the crust where they triggered melting leading to anatectic textures and the formation of the palites.

Conclusions

Zircon dating provides effective constraints on the early evolution of the Bavarian Pfahl shear zone. Syn-tectonic biotite-hornblende granitoids with large K-feldspar megacrysts (''palite'') show Lower Carboniferous U–Pb and Pb–Pb zircon ages. The rocks predate the thermal peak of the Upper Carboniferous low-pressure amphibolite facies regional metamorphism in the Bavarian Forest by about 10–15 Ma. Spatial association of the palites with the Pfahl zone suggests that their formation is closely linked to the initiation of the shear zone. Magma emplacement was facilitated by fracturing associated with the early shear zone activity, with in-situ lateral expansion. The shear zone acted as a localising conduit for the rise and entrapment of mantle melts into the surrounding crust driving the palite formation process.

The palites were subsequently intruded by granitic dykes and dyke injection was associated with penetrative mylonitisation. U–Pb age discordance caused by subsequent partial Pb loss causes a potential problem in determining the exact emplacement age of the dykes. U–Pb age discordance is found in particular in those fractions with high U content. Given the fact that the low U host rock zircons are concordant without exception, our data confirm earlier findings that metamictisation is the major driving force for the discordance of zircon. Upper discordia intercept ages between 326 and 331 Ma estimate the emplacement time of the dykes and thus define the maximum age of mylonitisation in the Bavarian Pfahl zone.

The petrologic history of the dyke and host-rock association is complex and not yet fully understood. The rocks preserve element signatures consistent with magmatic differentiation such as high-K calc-alkaline trend, decreasing Ti, Al, Fe, Mn, Ca, Mg, P and Sr concentration with increasing silica content. However, enhanced LREE and Th concentration in the dykes as well as evidence from Sr and Nd isotopes is difficult to explain with this concept. The set of presently available geochemical and isotopic data argue against a simple genetic relationship between palites and dykes.

Acknowledgements This paper has benefited from reviews by U. Schaltegger and an unknown reviewer. We wish to thank G. Bartholomä, O. Nzegge, E. Reitter, C. Shang and B. Steinhilber for help in preparing the mineral separates and isotopic measurements, H. Schulz for assistance at the scanning electron microscope, Ch. Berthold for photographic work and H. Taubald for XRF analyses.

References

Amelin YV, Heaman LM, Semenov VS (1995) U–Pb geochronology of layered mafic intrusions in the eastern Baltic Shield: implications for the timing and duration of Proterozoic continental rifting. Precambrian Res 75:31–46

Anczkiewicz R, Oberli F, Burg JP, Villa IM, Günther D, Meier M (2001) Timing of normal faulting along the Indus suture in Pakistan Himalaya and a case of major $^{231}Pa/^{235}U$ initial disequilibrium in zircon. Earth Planet Sci Lett 191:101–114

Brandmayr M, Dallmeyer RD, Handler R, Wallbrecher E (1995) Conjugate shear zones in the Southern Bohemian Massif (Austria): implications for Variscan and Alpine tectonothermal activity. Tectonophysics 248:97–116

Chen F, Siebel W, Satir M (2002a) Zircon U–Pb and Pb-isotope fractionation during stepwise HF-acid leaching and chronological implications. Chem Geol 191:155–164

Chen F, Siebel W, Satir M (2002b) Zircon geochronology and geochemistry of the Fürstenstein pluton, Bavarian Forest. Eur J Miner Bh 14(1):33

Chen F, Siebel W, Satir M, Terzioğlu MN, Saka K (2002c) Zircon geochronology and Nd–Sr isotope systematic in the Karadere basement (NW Turkey) and implications for the geological evolution of the Istanbul zone. Int J Earth Sci 45:431–456

Cherniak D, Watson EB (2000) Pb diffusion in zircon. Chem Geol 172:5–24

Cherniak D, Lanford W, Ryerson F (1991) Lead diffusion in apatite and zircon using ion implantation and Rutherford backscattering techniques. Geochim Cosmochim Acta 55:1663–1673

Christinas P, Köhler H, Müller-Sohnius D (1991) Altersstellung und Genese der Palite des Vorderen Bayerischen Waldes (Nordostbayern). Geol Bavarica 96:87–107

Cocherie A, Guerrot C, Rossi PH (1992) Single-zircon dating by step-wise Pb evaporation: comparison with other geochronological techniques applied to the Hercynian granites of Corsica, France. Chem Geol 101:131–141

Crowley JL (1999) U–Pb geochronologic constraints on Paleoproterozoic tectonism in the Monashee complex, Canadian Cordillera: elucidating an overprinted geologic history. Geol Soc Am Bull 111:560–577

Dvorak J (1985) Horizontal movements on deep faults in the Proterozoic basement of Moravia. Jahrb Geol Bundesanstalt Österreich 127:551–556

Fischer G (1938) Der Bayerische und der Böhmer Wald. Die Entwicklung seiner Landschaft im Laufe der geologischen Geschichte. Jahrb Preuß Geol Landesanstalt 59:355–382

Fischer G (1959) Der Bau des Vorderen Bayerischen Waldes. Jber Mitt Oberrh Geol Ver NF 41:1–22

Franke W (2000) The mid-European segment of the Variscides: tectonostratigraphic units, terrane boundaries and plate tectonic evolution. In: Franke W, Haak V, Oncken O, Tanner D (eds) Orogenic processes: quantification and modelling in the Variscan belt. Spec Publ Geol Soc Lond 179:35–61

Frentzel A (1911) Das Passauer Granitmassiv. Geognostisches Jahrb 24:31

Friedl G, von Quadt A, Finger F (1993) 340 Ma U/Pb-Monazitalter aus dem niederösterreichischen Moldanubikum und ihre geologische Bedeutung. Terra Nostra 3/94:43–46

Friedl G, von Quadt A, Ochsner A, Finger F (1994) Timing of the Variscan orogeny in the Southern Bohemian Massif (NE-Austria) deduced from new U–Pb zircon and monazite dating. Terra abstr 5:235–236

Gebauer D, Friedl G (1994) A 1.38 Ga protolith age for the Dobra orthogneiss (Moldanubian zone of the southern Bohemian Massif, NE Austria): evidence from ion-microprobe (SHRIMP) dating of zircon. J Czech Geol Soc 39:34–35

Gorz H (1974) Microprobe studies of inclusions in zircons and compilation of minor and trace elements in zircons from the literature. Chem Erde 33:326–357

Grauert B, Hänny R, Soptrajanova G (1974) Geochronology of a polymetamorphic anatectic gneiss region: the Moldanubicum of the area Lam-Deggendorf, eastern Bavaria, Germany. Contrib Mineral Petrol 45:37–63

Gümbel CW (1868) Geognostische Beschreibung des Königreiches Bayern. II. Abt. Ostbayerisches Grundgebirge, p 968 (Perthes)

Hanchar JM, Miller CF (1993) Zircon zonation patterns as revealed by cathodo-luminescence and backscattered electron images: implications for interpretation of complex crustal histories. Chem Geol 110:1–13

Hegemann F (1936) Über die Bildungsweise des Quarzes im Bayerischen Pfahl. Chem Erde 10:521–538

Hinton RW, Upton BGJ (1991) The chemistry of zircon: variations within and between large crystals from syenite and alkali basalt xenoliths. Geochim Cosmochim Acta 55:3287–3302

Hofmann R (1962) Die Tektonik des Bayerischen Pfahls. Geol Rundsch 52:332–346

Holl KP, von Drach V, Müller-Sohnius D, Köhler H (1989) Caledonian ages in Variscan rocks: Rb–Sr and Sm–Nd isotope variations in dioritic intrusives from the northwestern Bohemian Massif, West Germany. Tectonophysics 157:179–194

Horn P, Köhler H, Müller-Sohnius D (1986) Rb–Sr Isotopengeochemie hydrothermaler Quarze des Bayerischen Pfahls und eines Flußspat-Schwerspat-Ganges von Nabburg-Wölsendorf/Bundesrepublik Deutschland. Chem Geol 58:259–272

Janoušek V, Gerdes A (2003) Timing the magmatic activity within the Central Bohemian Pluton, Czech Republic: conventional U–Pb ages for the Sázava and Tábor intrusions and their geotectonic significance. J Czech Geol Soc 48(1–2):70–71

Kalt A, Corfu F, Wijbrans JR (2000) Time calibration of a P-T path from a Variscan high-temperature low-pressure metamorphic complex (Bayerische Wald, Germany), and the detection of inherited monazite. Contrib Mineral Petrol 138:143–163

Kamo SL, Krogh TE, Kamarapeli PS (1995) Age of the Grenville dyke swarm, Ontario-Quebec: implications for the timing of Lapetan rifting. Can J Earth Sci 32:273–280

Kempe U, Gruner T, Nasdala L, Wolf D (2000) Relevance of cathodoluminescence for the interpretation of U–Pb zircon ages, with an excample of an application to a study of zircons from the Saxonian granulite complex, Germany. In: Pagel M, Barbin V, Ohnenstetter D (eds) Cathodoluminescence in geosciences. Springer, Berlin Heidelberg New York, pp 415–455

Klötzli US (1999) Th/U zonation in zircon derived from evaporation analysis: a model and its implications. Chem Geol 158:325–333

Klötzli US, Parrish RR (1996) Zircon U/Pb and Pb/Pb geochronology of the Rastenberg granodiorite, South Bohemian Massif, Austria. Mineral Petrol 58:197–214

Kober B (1986) Whole-grain evaporation for $^{207}Pb/^{206}Pb$ age investigations on single zircons using a double-filament thermal ion source. Contrib Mineral Petrol 93:481–490

Kober B (1987) Single-zircon evaporation combined with Pb^{+} emitter-bedding for $^{207}Pb/^{206}Pb$-age investigations using thermal ion mass spectromerty, and implications to zirconology. Contrib Mineral Petrol 96:63–71

Köhler H, Propach G, Troll G (1989) Exkursion zur Geologie, Petrographie und Geochronologie des NE-bayerischen Grundgebirges. Ber Deutsch Mineral Ges 1(2):1–84

Košler J, Kelley SP, Vrána S (2001) $^{40}Ar/^{39}Ar$ hornblende dating of a microgranodiorite dyke: implications for early Permian extension in the Moldanubian zone of the Bohemian Massif. Int J Earth Sci 90:379–385

Krogh TE (1982) Improved accuracy of U-Pb zircon ages by the creation of more concordant systems using the air abrasion technique. Geochim Cosmochim Acta 46:637–649

Liew TC, Hofmann AW (1988) Precambrian crustal components, plutonic associations, plate environment of the Hercynian fold belt of central Europe: indications from a Nd and Sr isotopic study. Contrib Mineral Petrol 98:129–138

Ludwig KR (1988) PBdat for MS-Dos - a computer program for IBM-PC compatibles for processing raw Pb-U-Th isotope data. US Geol Surv, Open-file Report 88-542

Ludwig KR (2003) Isoplot 3.00—a geochronological toolkit for Microsoft Excel: Berkeley Geochronology Center, Special Publication No. 4

Matte P, Maluski H, Rajlich P, Franke W (1990) Terrane boundaries in the Bohemian Massif: result of large scale Variscan shearing. Tectonophysics 177:151–170

Mattern F (1995) Late Carboniferous to Lower Triassic shear sense reversals at strike-slip faults in eastern Bavaria. Zentralbl Geol Paläont Teil I 1993:1471–1490

Mattern F (2001) Permo-Silesian movements between Baltica and western Europe: tectonics and 'basin families'. Terra Nova 13:368–375

McDonough WF, Sun SS (1995) The composition of the Earth. Chem Geol 120:223–253

Meldrum A, Boatner LA, Weber WJ, Ewing RC (1998) Radiation damage in zircon and monazite. Geochim Cosmochim Acta 62:2509–2520

Mezger K, Krogstad EJ (1997) Interpretation of discordant U–Pb zircon ages: an evaluation. J Metamorphic Geol 15:127–140

Michael PJ (1984) Chemical differentiation of the Cordillera Paine granite (southern Chile) by in situ fractional crystallization. Contrib Mineral Petrol 87:179–195

Mielke H, Rohrmüller J, Gebauer D (1996) Ein metalateritisches Denudations-Niveau als lithologisch und zeitlich korrelierbarer Bezugshorizont in Phylliten, Glimmerschiefern und Gneisen des ostbayerischen Grundgebirges. Geol Bavarica 101:139–166

Miller CF, Mittlefehldt (1982) Depletion of light rare-earth elements in felsic magmas. Geology 10:129–133

Mulch A, Rosenau M, Dörr W, Handy MR (2002) The age and structure of dikes along the tectonic contact of the Ivrea-Verbano and Strona-Ceneri zones (southern Alps, Northern Italy, Switzerland). Schweiz Mineral Petrogr Mitt 82:55–76

Nagasawa H, Schnetzler CC (1971) Partitioning of rare earth, alkali and alkaline earth elements between phenocrysts and acidic igneous magmas. Geochim Cosmochim Acta 35:953–968

Nasdala L, Lengauer CL, Hanchar JM, Kronz A, Wirth R, Blanc P, Kennedy AK, Seydoux-Guillaume AM (2002) Annealing radiation damage and the recovery of cathodoluminescence. Chem Geol 191:121–140

Ochotzky H, Sandkühler B (1914) Zur Frage der Entstehung des Bayerischen Pfahles im Bayerischen Walde. Centralbl Mineral Geol Paläontol 1914:190

Petrakakis K (1997) Evolution of Moldanubian rocks in Austria: review and synthesis. J Metamorphic Geol 15:203–222

Peucker-Ehrenbrink B, Behr HJ (1993) Chemistry of hydrothermal quartz in the post-Variscan ''Bavarian Pfahl'' system, F.R. Germany. Chem Geol 103:85–102

Pidgeon RT, O'Neil JR, Silver LT (1966) Uranium and lead isotopic stability in a metamict zircon under experimental hydrothermal conditions. Science 154:1538–1540

Propach G, Baumann A, Schulz-Schmalschläger M, Grauert B (2000) Zircon and monazite U-Pb ages of Variscan granitoid rocks and gneisss in the Moldanubian zone of eastern Bavaria, Germany. Neues Jahrb Geol Paläontol Monatsh 2000(6):345–377

Rubatto D (2002) Zircon trace element geochemistry: partitioning with garnet and the link between U-Pb ages and metamorphism. Chem Geol 184:123–138

Rubatto D, Gebauer (2000) Use of cathodoluminescence for U-Pb zircon dating by ion microprobe: some examples from the western Alps. In: Pagel M, Barbin V, Ohnenstetter D (eds) Cathodoluminescence in geosciences. Springer, Berlin Heidelberg New York, pp 373–400

Schneider DA, Edwards MA, Zeitler PK, Coath CD (1999) Mazeno Pass pluton and Jutial pluton, Pakistan Himalaya: age and implications for entrapment mechanisms of two granites in the Himalaya. Contrib Mineral Petrol 136:273–284

Siebel W (1995) Anticorrelated Rb–Sr and K–Ar age discordances, Leuchtenberg granite, NE Bavaria, Germany. Contrib Mineral Petrol 120:197–211

Siebel W, Chen F, Satir M (2003) Late Variscan magmatism revisited: new implications from Pb-evaporation zircon ages on the emplacement of redwitzites and granites in NE Bavaria. Int J Earth Sci 92:36–53

Silver LT, Deutsch S (1963) Uranium-lead isotopic variations in zircons—a case study. J Geol 71:721–758

Sinha AK, Wayne DM, Hewitt DA (1992) The hydrothermal stability of zircon: preliminary experimental and isotopic studies. Geochim Cosmochim Acta 56:3551–3560

Stacey JS, Kramers JD (1975) Approximation of terrestrial lead isotope evolution by a two stage model. Earth Planet Sci Lett 26:207–221

Steiner L (1969) Kalifeldspatisierung in den Palitgesteinen des Pfahlgebietes. Geol Bavarica 60:163–169

Steiner L (1972) Alkalisierung im Grundgebirge des Bayerischen Waldes. Neues Jahrb Mineral Abh 116:132–166

Streckeisen AL (1976) Classification of the common igneous rocks by means of their chemical composition: a provisional attempt. Neues Jahrb Mineral Monatsh 1:1–15

Teipel U (2003) Obervendischer und unterordovizischer Magmatismus im Bayerischen Wald. Münchner Geol Hefte A33:98

Thiele O (1961) Zum Alter der Donaustörung. Verh Geol Bundesanstalt Österreich 1961:131–133

Troll G (1967) Die blastokataklastischen Kristallingesteine der Stallwanger Furche, Bayerischer Wald. Geol Bavarica 58:22–33

Wallbrecher E, Brandmayr M, Handler R. Loizenbauer J, Maderbacher F, Platzer R (1992) Konjugierende Scherzonen in der südlichen Böhmischen Masse: Variszische und alpidische kinematische Entwicklungen. Mitt Öster Mineral Ges 137:237–252

Weinberg RF (1996) Ascent mechanism of felsic magmas: news and views. Trans R Soc Edinburgh Earth Sci 87:95–103

White RS, Spence GD, Fowler SR, McKenzie DP, Westbrook GK, Bowen AN (1987) Magmatism at rifted continental margins. Nature 330:439–444

Woodhead JA, Rossman GR, Silver LT (1991) The metamictization of zircons: radiation dose dependent structural characteristics. Am Mineral 76:74–82

Zhang LS, Schärer U (1999) Age and origin of magmatism along the Cenozoic Red River shear belt, China. Contrib Mineral Petrol 134:67–85